

RESEARCH ARTICLE

The marine bacterium *Phaeobacter inhibens* secures external ammonium by rapid buildup of intracellular nitrogen stocks

Kathleen Trautwein¹, Michael Hensler², Katharina Wiegmann¹, Ekaterina Skorubskaya¹, Lars Wöhlbrand¹, Daniel Wünsch¹, Christina Hinrichs¹, Christoph Feenders³, Constanze Müller⁴, Kristina Schell¹, Hanna Ruppertsberg¹, Jannes Vagts¹, Sebastian Koßmehl¹, Alexander Steinbüchel⁵, Philippe Schmidt-Kopplin⁴, Heinz Wilkes⁶, Helmut Hillebrand^{7,8}, Bernd Blasius³, Dietmar Schomburg² and Ralf Rabus^{1,*}

¹General and Molecular Microbiology, Institute for Chemistry and Biology of the Marine Environment (ICBM), University Oldenburg, Carl-von-Ossietzky Str. 9-11, Oldenburg 26111, Germany, ²Bioinformatics and Biochemistry, Institute for Biochemistry and Biotechnology, Technische Universität Braunschweig, Rebenring 56, Braunschweig 38106, Germany, ³Mathematical Modelling, Institute for Chemistry and Biology of the Marine Environment (ICBM), University Oldenburg, Carl-von-Ossietzky Str. 9-11, Oldenburg 26111, Germany, ⁴Analytical BioGeoChemistry, HelmholtzZentrum München, German Research Centre for Environmental Health, Ingolstädter Landstr. 1, Neuherberg 85764, Germany, ⁵Institute for Molecular Microbiology and Biotechnology, WWU Münster, Corrensstr. 3, Münster 48149, Germany, ⁶Organic Geochemistry, Institute for Chemistry and Biology of the Marine Environment (ICBM), University Oldenburg, Carl-von-Ossietzky Str. 9-11, Oldenburg 26111, Germany, ⁷Planktology, Institute for Chemistry and Biology of the Marine Environment (ICBM), University Oldenburg, Carl-von-Ossietzky Str. 9-11, Oldenburg 26111, Germany and ⁸Helmholtz Institute for Functional Marine Biodiversity at the University of Oldenburg (HIFMB), Ammerländer Heerstr. 231, Oldenburg 23129, Germany

*Corresponding author: General and Molecular Microbiology, Institute for Chemistry and Biology of the Marine Environment (ICBM), University Oldenburg, Carl-von-Ossietzky Str. 9-11, Oldenburg 26111, Germany. Tel: +49 (0)441-798-3884; E-mail: rabus@icbm.de

One sentence summary: *Phaeobacter inhibens* DSM 17395 uncouples NH₄⁺-utilization from growth to build up a broad array of intracellular nitrogen stocks, paralleled by the secretion of RTX-like proteins and the antibiotic tropodithietic acid.

Editor: Tillmann Lueders

ABSTRACT

Received: 2 July 2017; Accepted: 13 August 2018

© FEMS 2018. This is an Open Access article distributed under the terms of the Creative Commons Attribution-NonCommercial-NoDerivs licence (<http://creativecommons.org/licenses/by-nc-nd/4.0/>), which permits non-commercial reproduction and distribution of the work, in any medium, provided the original work is not altered or transformed in any way, and that the work is properly cited. For commercial re-use, please contact journals.permissions@oup.com

Reduced nitrogen species are key nutrients for biological productivity in the oceans. Ammonium is often present in low and growth-limiting concentrations, albeit peaks occur during collapse of algal blooms or via input from deep sea upwelling and riverine inflow. Autotrophic phytoplankton exploit ammonium peaks by storing nitrogen intracellularly. In contrast, the strategy of heterotrophic bacterioplankton to acquire ammonium is less well understood. This study revealed the marine bacterium *Phaeobacter inhibens* DSM 17395, a *Roseobacter* group member, to have already depleted the external ammonium when only $\sim\frac{1}{3}$ of the ultimately attained biomass is formed. This was paralleled by a three-fold increase in cellular nitrogen levels and rapid buildup of various nitrogen-containing intracellular metabolites (and enzymes for their biosynthesis) and biopolymers (DNA, RNA and proteins). Moreover, nitrogen-rich cells secreted potential RTX proteins and the antibiotic tropodithetic acid, perhaps to competitively secure pulses of external ammonium and to protect themselves from predation. This complex response may ensure growing cells and their descendants exclusive provision with internal nitrogen stocks. This nutritional strategy appears prevalent also in other roseobacters from distant geographical provenances and could provide a new perspective on the distribution of reduced nitrogen in marine environments, i.e. temporary accumulation in bacterioplankton cells.

Keywords: *Phaeobacter inhibens* DSM 17395; *Roseobacter*; heterotrophic bacterioplankton; nitrogen storage; RTX proteins; tropodithetic acid

INTRODUCTION

A main originator of the elemental cycles in the world's oceans is the primary production accomplished by CO₂- and N₂-fixing phytoplankton and cyanobacteria. Their metabolic activity is responsible for about 50% of the global biomass production (Field et al. 1998) and also shapes the chemical composition of the ocean as conceptualized by the Redfield ratio (Redfield 1958). Transformation (to dissolved organic matter) and remineralization of about half of the net primary production is mainly executed by heterotrophic members of the bacterioplankton (microbial loop) in the sunlit euphotic zone (Azam and Malfatti 2007), even though a considerable share of the primary production is also exported via the biological pump to the deep sea (Laws et al. 2000). Nutrients are not homogeneously distributed across the oceanic water bodies, but range in a spatio-temporal manner from very low (e.g. in the open oceans) to high levels, e.g. in coastal, estuarine and upwelling regions (Falkowski, Barber and Smetacek 1998). The collapse of a seasonal phytoplankton bloom provides a regional nutrient pulse, triggering a dynamic succession of heterotrophic bacterioplankton populations with distinct metabolic proficiencies (Teeling et al. 2012).

The bioavailability of reduced nitrogen controls the productivity in the oceans to a large part (Zehr and Kudela 2011). While marine heterotrophic bacteria can utilize a large variety of different nitrogen sources (dissolved inorganic and organic nitrogen), ammonium (NH₄⁺) is the preferred inorganic nitrogen source as it can be readily incorporated into cell biomass during anabolism. In the euphotic zone, concentrations of NH₄⁺ are often in the low μM range, whereas it can be present at much higher concentrations in coastal and estuarine regions. Especially here, NH₄⁺ availability is expected to increase further owing to rising agricultural deposition (Li et al. 2016). Heterotrophic bacteria consume ~30% of the available NH₄⁺ and thereby compete with phytoplankton to exploit ephemeral peak supplies (Wheeler and Kirchman 1986; Kirchman 1994). The smaller sized bacteria grow faster and import NH₄⁺ more rapidly (Goldman and Dennett 2001), implicating a tight coupling of NH₄⁺ acquisition with growth and carbon source consumption, respectively (e.g. Goldman and Dennett 1991; Beg et al. 2012). In contrast, algae can uncouple growth from NH₄⁺ uptake due to their long known capacity for transient nitrogen storage (Dortch et al. 1984; Admiraal, Peletier and Laane 1986).

Roseobacters constitute a metabolically diverse group within the alphaproteobacterial *Rhodobacterales* and can account for ~20% of coastal and ~15% of mixed-layer ocean bacterioplankton communities. They inhabit coastal and open oceans, sea ice and the sea floor and occur planktonic as well as particle-associated (Buchan, González and Moran 2005; Wagner-Döbler and Biebl 2006). Notably, roseobacters were also found to associate with marine algae during phytoplankton blooms, thereby playing an important role in the recycling of seasonal peaks of phytoplankton-derived biomass (Teeling et al. 2012; Buchan et al. 2014; Luo and Moran 2014). A recent study examining effective population size as a measure of the adaptive potential suggested roseobacters to stay competitive in changing ocean habitats (Luo et al. 2014). The study organism, *Phaeobacter inhibens* DSM 17395, is a nutritionally versatile representative of roseobacters with a complex metabolism and regulation (Thole et al. 2012; Drüppel et al. 2014), and is apparently specialized for growth on biotic (e.g. algae) and abiotic surfaces in coastal areas (Gram et al. 2015).

A recent growth physiological study covering a wide concentration range of NH₄⁺ and PO₄³⁻ revealed *P. inhibens* DSM 17395 to be well adapted to fluctuating availability of inorganic N and P, and to grow optimally at N:P supply ratios (<50–120) markedly above Redfield (Trautwein et al. 2017). Considering the important role of NH₄⁺ for growth of *P. inhibens* DSM 17395 in particular and the general relevance of this macronutrient for the productivity of marine heterotrophic bacteria, the present study aims at investigating the NH₄⁺ acquisition and processing strategies of *P. inhibens* DSM 17395 as a well-studied representative of the *Roseobacter* group.

MATERIALS AND METHODS

Media, cultivation, sample retrieval and harvesting of cells

Phaeobacter inhibens DSM 17395 (originally deposited as *P. gallaeciensis* DSM 17395) (Buddruhs et al. 2013) was obtained from the Deutsche Sammlung von Mikroorganismen und Zellkulturen GmbH (DSMZ, Braunschweig, Germany) and maintained in our laboratory. Each growth experiment was started from a glycerol stock (stored at –80°C) prepared from cultures of *P. inhibens* DSM 17395 grown in marine broth (MB) medium. Revival of stock cultures proceeded in defined mineral medium supplemented with 11 mM glucose and residual glycerol/MB were eliminated by a dilution series (up to 10⁻⁵) (Zech et al. 2009). This was followed

by two successive passages in the same medium supplemented with different NH_4^+ concentrations (0.4, 0.8 or 1.8 mM; added from a sterile NH_4Cl stock solution). Each culture was inoculated with cells at the respective half-maximal optical density ($\sim \frac{1}{2} \text{OD}_{\text{max}}$). Cultivation was routinely performed in Erlenmeyer flasks (250 mL or 1 L), containing 50 or 250 mL of medium, respectively. All cultures were incubated on a rotary shaker (100 rpm) at 28°C in the dark and growth was monitored by measuring the OD at 600 nm (UVmini-1240; Shimadzu, Duisburg, Germany). All cultivation experiments and subsequent analyses are based on three to six biological replicates. Chemicals used were of analytical grade.

Selected bacterial strains from the marine bacterioplankton (Table S1, Supporting Information, 12 in total) as well as *Escherichia coli* were obtained from the DSMZ. Each strain was tested for growth under the identical cultivation conditions as described above for *P. inhibens* DSM 17395 (for further experimental details see Table S1, Supporting Information). The only exception was *E. coli* that was grown in standard M9 minimal medium (Sambrook and Russell 2001), accordingly supplemented with glucose and ammonium. In addition to four other roseobacters, only *R. blandensis* and *E. coli* grew reproducibly enough and sufficiently well in the used mineral media to perform detailed growth experiments.

Samples for the determination of NH_4^+ and glucose concentrations, as well as for flow cytometric analyses were retrieved from each culture in regular intervals. Each sample (1.8 mL culture broth) was centrifuged ($25,245 \times g$, 15 min, 4°C) and the supernatant transferred into new tubes. The samples for NH_4^+ determination were acidified with 10 μL of 0.1 M HCl. All samples were stored at -20°C until further analysis. For cellular dry weight (CDW), cultures were harvested by centrifugation ($11,300 \times g$, 20 min, 4°C), washed twice with 50 mM ammonium acetate and then resuspended in 300 μL 50 mM ammonium acetate and transferred into predried and weighed 1.5 mL tubes. The CDW was determined by gravimetric analysis of tubes after drying to constant weight at 60°C. Strong correlations ($R^2 \geq 0.96$) between OD and CDW were observed. CDW samples were stored at room temperature and used for determination of cellular carbon (C) and nitrogen (N) contents. To analyze the cellular composition (N-containing macromolecules), proteome, metabolome and lipidome, 3–6 replicate cultures (with 250 mL medium each) were harvested per sampling point and analysis type from 14 to 96 h after inoculation in order to cover all growth phases. Reproducible growth of each harvested culture was controlled by continued incubation of a 20 mL subculture transferred to 100 mL Erlenmeyer flasks prior to harvesting. At low ODs, several cultures were pooled to obtain sufficient cell material for chemical and compositional analyses of biomass. Cell harvesting included centrifugation ($14,300 \times g$, 20 min, 4°C) and washing steps specific for the various analysis types: cell pellets for (i) chemical analysis of biomass (aliquoted to cell pellets of 1, 2 and 5 mg dry cells) were washed twice with 3.7% (w/v) NaCl, (ii) proteome analysis were washed twice with Tris/HCl buffer (100 mM Tris, 5 mM $\text{MgCl}_2 \times 6 \text{H}_2\text{O}$, adjusted to pH 7.5) and (iii) analysis of the intracellular metabolome or lipidome were washed twice with 3.7 or 0.9% (w/v) NaCl, respectively. Each cell pellet was immediately shock frozen in liquid N_2 and stored at -80°C until further analysis. Samples (5–96 h after inoculation) for analysis of the exoproteome (200 or 400 mL) were retrieved from the culture supernatant after the first centrifugation step, immediately filtered (0.2 μm CA; Sartorius, Göttingen, Germany), and then directly processed (see below).

Chemical analyses

The concentration of NH_4^+ in cell-free culture supernatants was determined according to the method reported by Chaney and Marbach (1962). For calibration of the assay, 0–200 μM NH_4Cl was dissolved in defined (NH_4^+ -free) mineral medium. The procedure of the assay was as follows: 800 μL of sample or calibration standard were placed in 1.5 mL reaction tubes and 100 μL reagent A (3 g phenol, 3 mg sodium nitroprusside; both dissolved in 100 mL H_2O , final pH 5.3; stored for up to 2 weeks at 4°C–8°C) were added. After mixing, 100 μL of reagent B (2 g NaOH, 0.5 mL 13% (w/v) NaOCl; dissolved in 100 mL H_2O , final pH 13.5; stored at 4°C–8°C) were added. Following further mixing, the assay mixture was incubated at room temperature for 1 h in the dark and then centrifuged ($20,000 \times g$, 4°C, 1 min). The supernatant was transferred into a cuvette and the absorption was measured at 635 nm (UVmini-1240). The limit of quantitation was 5.1 μM . The assay was adapted to lower sample volumes and higher throughput (96-well plates) by employing a microplate reader (FLUOstar OPTIMA; BMG Labtech GmbH, Ortenberg, Germany) (Ruppersberg et al. 2017). The limit of quantitation in this case was 36 μM NH_4^+ .

The concentration of glucose in cell-free culture supernatants was determined by HPLC analysis. The system consisted of an UltiMate 3000 Rapid Separation LC (ThermoFisher Scientific, Germering, Germany) equipped with a Eurokat separation column (8 \times 300 mm, 10 μm bead size; Knauer, Berlin, Germany) temperature controlled at 75°C and a refractive index (RI) detector. The eluent was composed of 5 mM H_2SO_4 and administered at a flow rate of 1.2 mL min^{-1} . Calibration was performed with a glucose standard (retention time at 8 min) diluted in mineral medium ranging from 0.01 to 15 mM.

The cellular C and N content was determined by subjecting samples (1–5 mg dry cells) to high temperature oxidation, sequential heat-dependent release from adsorption columns and thermal conductivity detection using a Vario EL cube (Elementar Analysensysteme GmbH, Hanau, Germany) essentially as described before (Zech et al. 2013a).

The cellular content of DNA or RNA was quantified independently in cell pellets with the ‘Genomic DNA from tissue kit’ or the ‘NucleoSpin RNA kit’ following the manufacturer’s instructions (both from Macherey–Nagel, Düren, Germany). Isolated nucleic acids were measured spectrophotometrically in a tray cell (Hellma, Müllheim, Germany) at 230, 260 and 280 nm (UV-1800; Shimadzu) to determine the concentration and purity of DNA and RNA. The cellular protein content was quantified in cell pellets after alkaline lysis of cells in 0.5 M NaOH and 2% (w/v) SDS for 10 min at 95°C in a thermoblock mixing at 600 rpm. This was followed by a 10 min incubation in an ultrasonic bath at 60°C, and centrifugation of the lysate ($20,000 \times g$, 5 min, 20°C). The protein concentration in the supernatant was determined with the RC DC Protein Assay Kit II (BioRad, Munich, Germany) according to the manufacturer’s instructions, using bovine serum albumin (BSA; Sigma-Aldrich, Hamburg, Germany) as calibration standard. Each of four biological replicate samples for DNA, RNA and protein was measured three times.

Poly(3-hydroxybutanoate) (PHB) was analyzed in cell pellets (5–10 mg dry weight each) essentially as described (Trautwein et al. 2008). The total amount of PHB was quantified by GC in relation to methyl esters obtained from purchased sodium salt of 3-hydroxybutanoic acid.

The concentration of tropodithietic acid (TDA) was estimated using an indirect spectrophotometric assay that is based on the reported color shift (from transparent to brown) upon binding of TDA to ferric/ferrous iron present in the medium (D'Alvise et al. 2015).

Flow cytometry

The DNA, RNA, protein and PHB content of cells was also determined with a FACSCalibur flow cytometer (Becton Dickinson, Franklin Lakes, NJ, USA). Immediately after sample retrieval, cells were fixed with formaldehyde and after several washing steps, stored at -20°C (Trautwein et al. 2012). Fixed cells were diluted 1:150 in phosphate-buffered saline (PBS) (145 mM NaCl, 8 mM Na_2HPO_4 , 1.4 mM NaH_2PO_4 , adjusted to pH 7.4) and stained with SYBR green I (for DNA; Molecular Probes, Eugene, OR, USA), SYTO RNASelect green fluorescent cell stain (for RNA; Molecular Probes), Flamingo (for proteins; Bio-Rad) or Nile red (for PHBs; Sigma-Aldrich). Nile red (final concentration $5\ \mu\text{g mL}^{-1}$) staining was carried out at room temperature in the dark for 30 min. If necessary, samples were further diluted 1:2 with PBS prior to analysis. Measurements (irrespective of the type of staining) were standardized to the fluorescence of suitable fluorescent latex beads (pink or yellow-green; Molecular Probes) added to each sample prior to analysis. A total of 70,000 (40,000 only at very low cell densities) events were recorded per measurement, and each sample (3–4 biological replicates per sampling point) was measured in triplicate. Data acquisition and analysis were performed with CellQuest Pro software (Becton Dickinson). Data analysis was manually controlled for each sample and included $\sim 85\%$ – 90% of the total cell events (core population) to reduce the influence of morphological changes of a minor cell fraction during growth on average fluorescence values.

Proteomic analyses

The proteomic strategy targeted intracellular soluble (by 2D DIGE and whole cell shotgun analysis), membrane and extracellular proteins. Protein concentrations in the soluble intra- and extracellular protein fractions were determined with the method described by Bradford (1976), while that introduced by Lowry et al. (1951) was used for the membrane proteins (RC DC Protein Assay Kit II; Bio-Rad). In both cases, BSA (Sigma-Aldrich) was used as calibration standard.

2D DIGE

Cell pellets (from 4–6 independent cultures per sampling point) of *P. inhibens* DSM 17395 were resuspended in 1 mL lysis buffer (7 M urea, 2 M thiourea, 30 mM Tris, 4% CHAPS; final pH 8.5) and cells were disrupted using the Plus One Sample Grinding Kit (GE Healthcare, Munich, Germany) as described by Gade et al. (2003). The pre-electrophoretic labeling with CyDyes (GE Healthcare) was carried out as described before (Gade et al. 2003), with the exception that 50 μg of each protein sample were labeled with 200 pmol of commercial fluorescent dye (Drüppel et al. 2014). In the present study, protein extracts of cells harvested 30 h after inoculation served as reference state and were labeled with Cy5. Protein extracts of cells harvested at all other sampling points served as individual test states and were each labeled with Cy3. The internal standard was composed of equal amounts of all protein extracts and was labeled with Cy2. Isoelectric focusing (IEF) was carried out as previously described (Zech et al. 2009), employing a combination of narrow (3–5.6) and wide (3–11) range non-linear (NL) pH gradients (IPG strips, 24 cm; GE Healthcare)

and a protein load of 150 μg protein per IPG strip. Equilibration of IPG strips with buffers containing dithiothreitol (DTT) or iodoacetamide was performed as described by Görg, Weiss and Dunn (2004). Second dimension protein separation was achieved with 12.5% (v/v) acrylamide gels and the EttanDalt II system (GE Healthcare) as described before (Gade et al. 2003). Samples from four independent cultures (biological replicates) were analyzed per sampling point.

2D DIGE gels were digitalized with a Typhoon 9400 laser scanner (GE Healthcare) set to a resolution of 100 μm . Gel images were cropped with the ImageQuant software (version 7.0; GE Healthcare) to obtain good alignment between the pH 5–11 (from pH 3–11 gel) and the pH 3–5.6 regions. Cropped gel images were sorted into two different work packages (pH 3–5.6 or pH 5–11) for image analysis with the DeCyder 2D software (version 7.0; GE Healthcare), which was performed as described previously (Zech et al. 2009). Differentially abundant protein spots had to fulfill the following criteria: average ratio (fold change in protein abundance) of ≤ -1.5 or ≥ 1.5 , ANOVA *p*-value of < 0.05 , *t*-test value of $< 10^{-4}$ and matched in at least 75% of the gel images in the work package.

Protein spots with changed abundances were excised with the EXQuest spot cutter (Bio-Rad) from separate, preparative 2DE gels (300 μg protein load) stained with colloidal Coomassie Brilliant Blue (cCBB) (Doherty et al. 1998). Each protein spot was excised from two replicate gels and processed independently. Subsequent washing steps, in-gel tryptic digestion, spotting onto Anchorchip steel targets (Bruker Daltonik GmbH, Bremen, Germany) and mass spectrometric analysis with an UltrafleXtreme MALDI-TOF/TOF mass spectrometer (Bruker Daltonik GmbH) was performed as described recently (Košmehl et al. 2013). Proteins were identified by PMF and PFF mapping, respectively, using an in-house Mascot server (version 2.3; Matrix Science, London, UK) via the ProteinScape platform (version 3.1; Bruker Daltonik GmbH). Acquired MS and MS/MS spectra were searched against the translated genome of *P. inhibens* DSM 17395 (Thole et al. 2012) as described by Košmehl et al. (2013).

Whole cell shotgun

Samples from three independent cultures were subjected to shotgun proteomic analysis per sampling point. Essentially, suspending cell pellets in lysis buffer (7 M urea, 2 M thiourea, 30 mM Tris, pH 8.5), cell breakage, removal of cell debris, reduction with DTT, alkylation with iodoacetamide and tryptic in-solution digestion were performed as described previously (Zech et al. 2013a). Total peptide mixtures were separated with an Ultimate 3000 nanoRSLC system (ThermoFisher Scientific) in a trap column setup equipped with an analytical column (C_{18} ; pore size, 100 Å; bead size, 2 μm ; inner diameter, 75 μm ; length, 25 cm; ThermoFisher Scientific), as previously described (Zech et al. 2013a). Continuous analysis of the eluent was performed with an online-coupled electrospray ion source (captive spray; Bruker Daltonik GmbH) ion trap mass spectrometer (amazon ETD; Bruker Daltonik GmbH) operated in positive mode with a capillary current of 1.3 kV and dry gas flow of 3 L min^{-1} at 150°C . Per full scan MS, 20 MS/MS spectra of most intense masses were acquired. Active precursor exclusion was set for 0.2 min. Protein identification was performed with ProteinScape as described above, allowing for a mass difference of 0.3 Da and applying a target decoy strategy (false discovery rate $< 1\%$).

Membrane proteins

Membrane protein-enriched cell fractions were prepared from two biological replicates per sampling point. Preparation of

membrane proteins involved cell disruption by French Press (Sim-Aminco Ltd., Rochester, NY, USA), treatment with ice-cold carbonate and solubilization of membrane proteins with hot SDS as previously described (Trautwein et al. 2012; Koßmehl et al. 2013). Electrophoretic separation of similar amounts of membrane proteins was conducted with 7 cm long, 1 mm thick 12.5% (v/v) SDS-PAGE gels using the Mini-Protean Tetra System (Bio-Rad) (Zech et al. 2013a). Gels were stained with cCBB and following digitalization, each sample lane (from two different gels) was cut into four slices. Each slice was then cut into ~ 1 mm³ pieces, which were washed, reduced, alkylated and tryptically digested as described (Zech et al. 2013a). Separation of peptide mixtures and mass spectrometric analysis were performed with a nanoLC-ESI-MS/MS system and protein identification by means of the ProteinScape platform as described above for the shotgun analysis of soluble proteins.

Exoproteins

Extracellular proteins were precipitated by addition of trichloroacetic acid (final concentration 10% (v/v)) added to the filtered culture supernatants (200 or 400 mL) directly after centrifugation. After incubation for 12–14 h at 4°C, the precipitated proteins were collected by centrifugation (17,700 \times g, 1 h, 4°C) and washed six times with 1 mL 96% (v/v) ethanol (20,000 g, 15 min, 4°C). The protein pellets were dried and immediately resuspended in 400 μ L lysis buffer (pH adjusted to 8.0). One final round of centrifugation (20,817 g, 10 min, 12°C) was carried out to remove insoluble material. Protein extracts were aliquoted, then immediately frozen in liquid N₂ and stored at -80°C . Proteins were quantified (Bradford 1976) and similar amounts were separated by SDS PAGE on four separate gels that were stained with cCBB. Following the digitalization of gels with the GS-800 Calibrated Densitometer (Bio-Rad), each sample lane (from two different gels) was cut into eight slices. Further processing of gel slices, separation of peptide mixtures and mass spectrometric analysis were performed as described above for membrane proteins. The four digital gel images were analyzed with the Quantity One software (version 4.6.9; Bio-Rad) according to the manufacturer's instructions to quantify intensity changes of protein bands in the exoproteome during growth.

Intracellular metabolome

Five to six samples per harvesting time point were prepared for gas chromatography-mass spectrometry (GC-MS) analysis as previously described (Zech et al. 2013a). Essentially, cell pellets were resuspended in 1.5 mL of ribitol-containing ethanol and cell breakage was achieved by ultra-sonication. Following removal of hydrophobic compounds by extraction with chloroform and centrifugation (3900 \times g, 5 min, 4°C), samples were dried and stored at -20°C . Prior to analysis, samples were derivatized according to the two-step procedure previously described (Zech et al. 2009). Essentially, samples were first treated with methoxyamine hydrochloride and then silylated using *N*-methyl-*N*-(trimethylsilyl)-trifluoroacetamide (MSTFA).

Derivatized samples were analyzed using a Leco Pegasus 4d GC \times GC TOF mass spectrometer (Leco Instrumente, Mönchengladbach, Germany). The instrument was operated in GC-TOF mode, equipped with a MPS 2 XL autosampler connected to a programmed temperature vaporizing (PTV) injector (Gerstel, Mülheim a.d. Ruhr, Germany) and calibrated with

perfluorotributylamine. Samples (1 μ L) were injected in splitless mode and vaporized along the following temperature profile: 70°C for 0.02 min, ramping by 12°C s⁻¹ to 330°C, and then constant for 5 min. The GC instrument (7890 Agilent GC; Agilent, Santa Clara, USA) was equipped with a ZB-5MS column (particle size, 25 μ m; length, 30 m; inner diameter 0.25 mm; Phenomenex, Aschaffenburg, Germany) operated with helium (1.2 mL min⁻¹) and the following temperature profile: 70°C for 1 min, ramping by 10°C s⁻¹ to 330°C, and then constant for 3 min. The transfer line to the mass spectrometer was set to 275°C, the ion source to 250°C and the detector voltage 200 V higher than the output of the automatic tuning. Following a solvent delay of around 300 s, full mass spectra were collected from 45 to 600 *m/z* at 8 scans s⁻¹ using the ChromaTOF software (version 4.24; Leco Instrumente).

Data analysis was done with the Metabolite Detector software (Hiller et al. 2009) as described before (Zech et al. 2009) and included normalization by the internal standard ribitol and cell mass.

Lipidome

Bacterial cell mass was reconstituted in 1.5 mL methanol; 5 mL of methyl-*tert*-butyl ether (MTBE) was added and lipid extraction was performed for 1 h in an ultra-sonic bath on ice (Matyash et al. 2008). The organic solvents were evaporated and the samples were reconstituted in methanol directly before measurement.

The crude lipid extracts were analyzed by a UPLC-qTOF mass spectrometer (Acquity UPLC; Waters, Milford, USA; maxis MS, Bruker Daltonik GmbH) using a Cortecs UPLC C₁₈ column (pore size, 90 Å; particle size, 1.6 μ m; length 150 mm; inner diameter, 2.1 mm; Waters) and applying 1.5 min isocratic elution at 32% B, followed by a gradient leading to 97% B in 21 min (solvent A: 60/40 acetonitrile/water, 10 mM ammonium formate, 0.1% formic acid; solvent B: 90/10 *n*-propanol/acetonitrile, 10 mM ammonium formate, 0.1% formic acid) and a 4 min plateau at 9% B (column temperature 40°C, sample temperature 5°C, flow 0.225 mL min⁻¹, injection volume 10 μ L). Mass spectra were acquired in positive electrospray mode. Parameters of the qTOF instrument were set for best resolution and mass accuracy in the mass range of approximately 500–900 Da. Analysis of a phospholipids standard solution was included in the analytical workflow as quality control (Boncompain et al. 2014). Genedata Refiner (Genedata AG, Basel, Switzerland) was applied for chromatographic and mass spectrometric calibration and alignment. 2656 lipid clusters were detected, for which MassTRIX annotation (Suhre and Schmitt-Kopplin 2008) (max. error <0.01 Da) was performed. Statistical analysis was done in Genedata Analyst (Genedata), Simca P (Umetrics, Malmö, Sweden) and HCE 3.0 (Human-Computer Interaction Lab, Maryland, MD, USA).

Identification was achieved by MS² experiments using either targeted quadrupole extraction for lipid species containing nitrogen and showing a decreasing abundance over incubation time or in auto MS mode at 40 eV, resulting in fragmentation of the dominant ion species.

Modeling

A cell population model was fitted to experimentally determined values for OD, NH₄⁺ and glucose concentrations, as well as to N:P ratios of biomass. The applied model described by Droop (1968) was adopted to include the relevant solute uptake systems for NH₄⁺ and glucose, respectively. NH₄⁺ uptake is described by

Monod kinetics (Monod 1942) as follows

$$\rho^a(A) = \frac{\rho_{max}^a A}{\rho_S^a + A}$$

with NH_4^+ concentration A , maximum uptake rate ρ_{max}^a , and half-saturation constant ρ_S^a . Glucose uptake $\rho^g(G)$ is described analogously with glucose concentration G , maximum uptake rate ρ_{max}^g and half-saturation constant ρ_S^g .

The modified Droop equations (see below) were applied to describe the dynamics of the bacterial population in the batch culture: the population density P , extracellular NH_4^+ concentration A , extracellular glucose concentration G and cell quota Q (reflecting the nitrogen content per cell) vary according to

$$\dot{P} = [\mu(Q, G) - m] P$$

$$\dot{A} = -\rho^a(A) P$$

$$\dot{G} = -\beta \mu(Q, G) P$$

$$\dot{Q} = \rho^a(A) - \alpha \mu(Q, G) Q$$

where

$$\mu(Q, G) = \min \{ \mu_A(Q), \mu_G(G) \}$$

$$\mu_A(Q) = \mu_{max}^A \left[1 - \frac{Q_{min}}{Q} \right]$$

$$\mu_G(G) = \frac{\rho_G(G)}{\beta}$$

with conversion coefficients α and β , mortality m , maximal quota-dependent growth μ_{max}^A and minimum quota Q_{min} . The variable growth rate $\mu(Q, G)$ implements Liebig's law of the minimum, selecting either growth rate $\mu_A(Q)$, which depends on the nitrogen cell quota Q , or glucose-dependent growth rate $\mu_G(G)$ if smaller.

Model parameters (Table S2, Supporting Information) were determined by minimizing the sum of relative mean deviations between experimental data and model simulations (i.e. OD and P , NH_4^+ and A , glucose and G , N:P ratio and Q) using the metaheuristics differential evolution (Storn and Price 1997) and adaptive simulated annealing (Ingber 1989) implemented by Oldenhuis and Vandekerckhove (2009).

Genomic analysis

The genome sequence of *P. inhibens* DSM 17395 (Thole et al. 2012) served as backbone for integrated metabolic reconstruction based on proteomic and metabolomic data. FunPhaeobacterctional assignments for potential transport proteins were based on the Transporter Classification Database (TCDB) (Saier et al. 2016). Metabolic pathways were assessed with BRENDA (Chang et al. 2015) and MetaCyc (Caspi et al. 2016).

RESULTS AND DISCUSSION

Phaeobacter inhibens DSM 17395 rapidly depletes external ammonium and increases the cellular N:C ratio

In growth experiments with marine mineral medium, *P. inhibens* DSM 17395 rapidly and completely depleted the nitrogen source supplied (0.8 mM NH_4^+) during early (exponential) growth, i.e. when only low ($\sim \frac{1}{3}$ of maximal) biomass concentrations were formed (Fig. 1a). This marked uncoupling of NH_4^+ consumption from bulk (linear) growth suggests that *P. inhibens* DSM 17395 accumulates reduced nitrogen during early growth (≤ 20 h).

The buildup of intracellular nitrogen reservoirs is evident from cellular N:C ratios (Fig. 1b), increasing from ~ 0.09 (inoculum) to maximal values of ~ 0.22 within less than 10 h ($\sim 10\%$ NH_4^+ depleted) and then remained constant for 5–6 h during bulk NH_4^+ depletion. Subsequently, N:C ratios decreased continuously until a constant minimal level of ~ 0.06 was reached at the transition into the stationary growth phase (~ 50 h after inoculation), marking the onset of nitrogen starvation. Varying the concentration of initially supplied NH_4^+ , i.e. more limiting (0.4 mM) or excess (1.8 mM), revealed very similar N:C ratio profiles (Fig. S1, Supporting Information), thus indicating that molecular crowding and solvation/diffusion capacities could constrain elemental homeostasis and therefore the upper limit (N:C ratios of 0.22–0.24). The low N:C ratios (0.06) of *P. inhibens* DSM 17395 during the stationary growth phase agree with growth limitation by nitrogen and storage of carbon as PHB, the formation of which started upon depletion of external NH_4^+ (Fig. 1f). The nutrient quota (Droop 1968) modeled for nitrogen complies with profiles of cellular N:C ratios in *P. inhibens* DSM 17395 (Fig. 1b; Fig. S2, Supporting Information). The initially high quota reflects the storage of nitrogen during NH_4^+ depletion, followed by its decrease due to allocation of internal nitrogen pools to descending cells during cell division.

The marked uncoupling of NH_4^+ consumption from bulk growth by *P. inhibens* DSM 17395 is noteworthy, as previous reports showed *Klebsiella pneumoniae* to tightly couple NH_4^+ consumption with growth under similar cultivation condition, i.e. growth ceased upon NH_4^+ depletion from the medium (Wanner and Egli 1990). Subsequent slow and slight increases in biomass observed for *K. pneumoniae* and other bacteria (e.g. *E. coli*, *Aerobacter aerogenes*) result from conversion of excess carbon source into storage polymers, rather than from growth *per se* (Duguid and Wilkinson 1953; Wanner and Egli 1990; Guevara-Martinez et al. 2015). In contrast, it is long known that utilization of phosphate, another macronutrient, can be decoupled from growth in *K. pneumoniae* and *E. coli*, with elevated levels of DNA and RNA serving as phosphate storage to sustain successive growth (Horiuchi 1959; Wanner and Egli 1990).

Rapid nitrogen storage prevalent in other *Phaeobacter* spp. and *Ruegeria pomeroyi*

Recent metagenomic studies revealed that *Phaeobacter* and *Ruegeria* spp. constitute a major fraction of the roseobacters associating with large-scale blooms of the widespread marine coccolithophore *Emiliana huxleyi* (Segev et al. 2016). Further tested strains of *P. inhibens*, *P. gallaeciensis* and *R. pomeroyi* exploited external NH_4^+ essentially as observed for *P. inhibens* DSM 17395 (Fig. 1), i.e. they uncoupled NH_4^+ depletion from bulk growth and at the same time increased the cellular N:C ratio (Fig. 2; Fig. S3, Supporting Information). Potential eco-

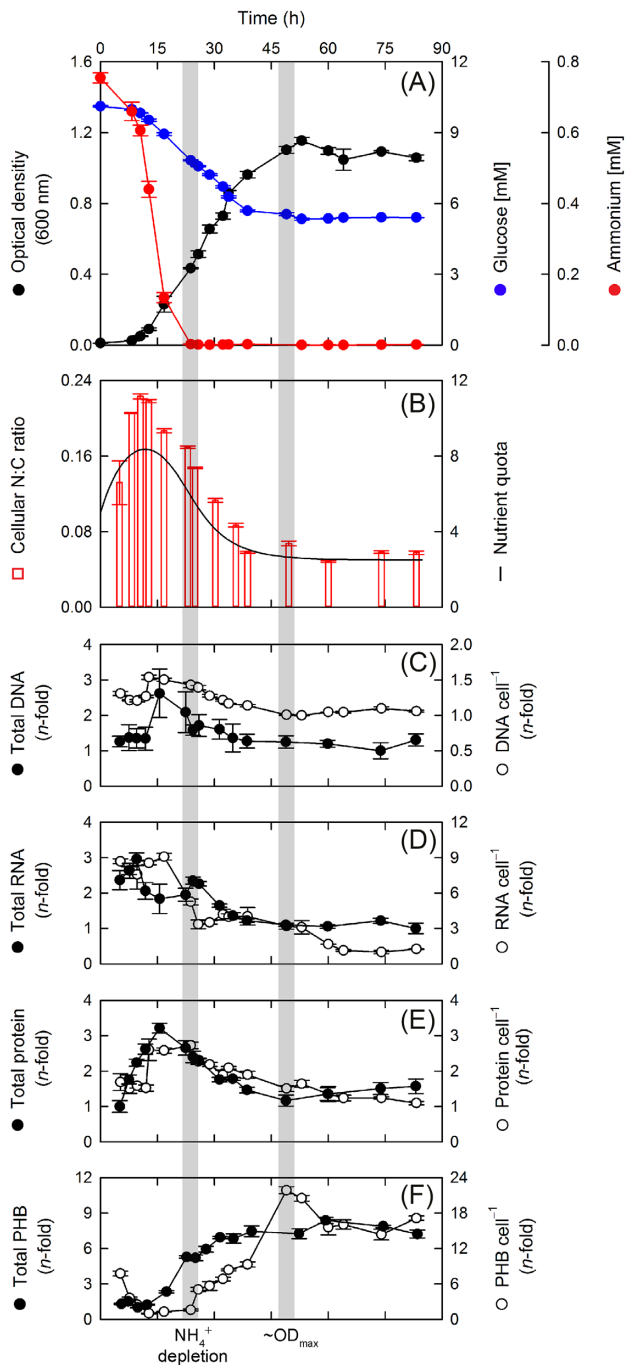


Figure 1. Ammonium assimilation is uncoupled from growth in *P. inhibens* DSM 17395 and accompanied by the buildup of intracellular nitrogen stocks. (A) Growth and substrate consumption profiles with 0.8 mM ammonium provided as sole nitrogen source in glucose-containing seawater medium. (B) Cellular (molar) N:C ratios determined by chemical analysis and modeled nutrient quota (Fig. S2, Supporting Information). (C–F) Abundance profiles of N-containing cellular macromolecules including (C) DNA, (D) RNA, and (E) proteins as well as for (F) the carbon reserve polymer PHB. For complementary metabolite abundances of the PHB monomer 3-hydroxybutanoate see Table S4, Supporting Information. Biopolymers were determined in total biomass (by chemical analysis; filled symbols) and in single cells (by flow cytometry; open symbols). The *n*-fold change relates each data point to the lowest measured value of the respective dataset. Displayed data (average \pm average deviation) are based on 3–4 biological replicates. The provision with different concentrations of NH_4^+ (Fig. S1, Supporting Information) or trace elements (Fig. S9, Supporting Information) had no effect on the observed uncoupling of ammonium depletion from growth.

physiological relevance of this nutritional strategy may be inferred from the distant geographic provenances of the studied strains (Fig. 2). This ammonium acquisition and storage strategy was not observed with gammaproteobacterial *Reinekea blandensis* (marine) and *E. coli* (human gut). In contrast to the five roseobacters, *R. blandensis* and *E. coli* completely depleted external NH_4^+ at ~ 61 – 63% of OD_{max} (vs. 16%–39% for the roseobacters) and increased their cellular N:C ratios at 50% NH_4^+ depletion only slightly by ~ 1.4 – 1.5 -fold (vs. 2.7–4.5-fold for the roseobacters) (Fig. 2; Fig. S3, Supporting Information).

The determined cellular N:C ratios are within the wide range of values (0.07 to 0.35) observed for marine bacteria (Fagerbakke, Haldal and Norland 1996), reflecting the heterogeneous nitrogen availability in the oceans, as well as species- and growth phase-specific differences in nitrogen requirements. The capacity to store nitrogen internally during transient pulses of NH_4^+ or nitrate is a typical feature of marine phytoplankton (Dortch et al. 1984; Admiraal, Peletier and Laane 1986) and was recently also observed in the cyanobacterium *Planktothrix agardhii* (Van de Waal et al. 2010), but has to our knowledge not been reported for heterotrophic bacterioplankton members.

Chemical identity of intracellular nitrogen species buildup by *P. inhibens* DSM 17395 during early growth

Uptake of NH_4^+ by *P. inhibens* DSM 17395 during early growth is apparently facilitated by the AmtB family transporter PGA1.c29410 (identified; Table S3, Supporting Information), regulated by its cognate P_{II} family protein GlnK (identified) (Thomas, Coutts and Merrick 2000; Conroy et al. 2007). The proteomic and metabolomic datasets (Tables S3 and S4, Supporting Information) indicated that *P. inhibens* DSM 17395 rapidly assimilated the imported NH_4^+ via the canonical pathways (glutamate dehydrogenase GluD, glutamine-forming glutamate synthase GltBD and several aminotransferases). Nitrogen assimilation resulted in the buildup of manifold nitrogen-containing small metabolites (Fig. 3), with most of them serving as building blocks for the biosynthesis of cellular macromolecules (Fig. 1).

Amino acids and their derivatives represented the largest group of intracellular metabolites formed during depletion of external NH_4^+ (Fig. 3). Relative abundances of individual amino acids in *P. inhibens* DSM 17395 (Table S4, Supporting Information) reflected their distribution known to universally occur in living cells. In accord, particularly high abundance increases (up to ~ 20 -fold) were detected for branched-chain amino acids (Leu, Val, Ile), which was paralleled by the presence of the corresponding enzymes for their biosynthesis (mostly) also at elevated levels (Fig. S4, Supporting Information). Additional strongly elevated N-containing metabolites comprised three nucleotides (C, T, U), six carboxylates (e.g. 4-aminobutanoate), the biogenic amine putrescine, the amino alcohol diethanolamine and the dipeptide glycyl-glycine (Fig. 3). Among cellular lipids, N-containing glycerol phospholipids (phosphatidylcholine, phosphatidylethanolamine) contributed only a minor fraction (Fig. S5, Supporting Information). The rapid assimilation of imported NH_4^+ by *P. inhibens* DSM 17395 avoids futile cycling of $\text{NH}_3/\text{NH}_4^+$ across the cytoplasmic membrane (Kleiner 1985), and thus energy wastage. Nevertheless, boosting the costly biosynthesis of the many and diverse nitrogen-containing metabolites required massive production of the respective enzymes (Table S3, Supporting Information), presupposing global changes in gene expression in response to external NH_4^+ . For this purpose, the formed NtrBC/ P_{II} and P_{II} -independent NtrXY systems (Table

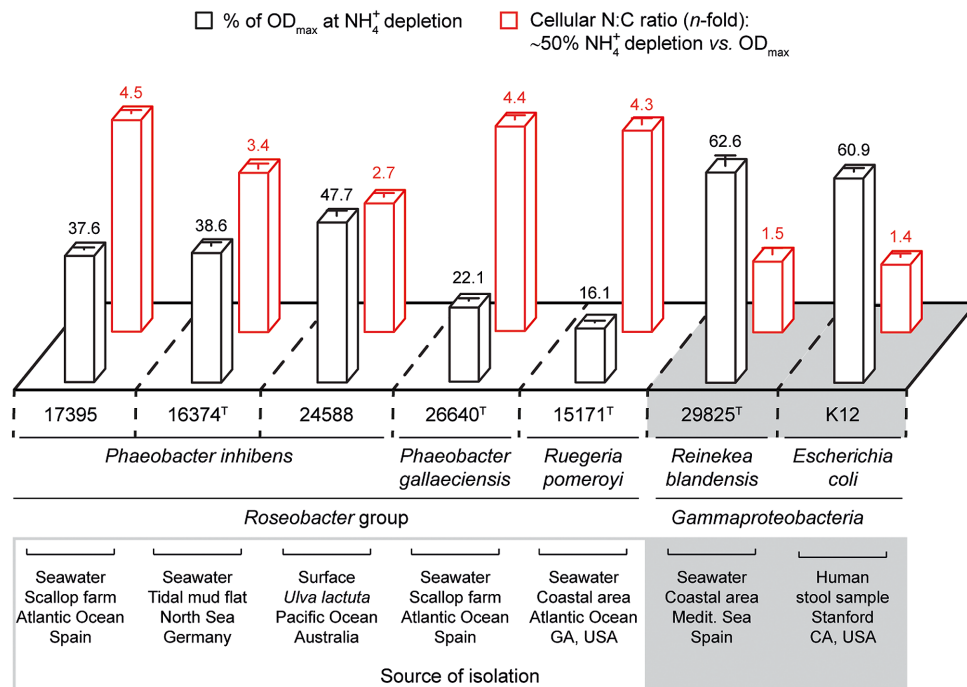


Figure 2. Rapid nitrogen storage prevalent in other *Phaeobacter* spp. and *Ruegeria pomeroyi*. Uncoupling of bulk growth from NH₄⁺ depletion was detected also in other roseobacters that were cultivable in the same mineral medium as used for *P. inhibens* DSM 17395 (see Fig. 1). All strains had already depleted NH₄⁺ completely when only 16.1%–47.7% of the maximal optical densities (OD_{max}) were attained. During NH₄⁺ depletion (at ~50% consumed), all strains buildup intracellular nitrogen stocks, as evidenced by the 2.7–4.5-fold increase in cellular N:C ratios (in comparison to cells at OD_{max}). The non-Roseobacter strains *R. blandensis* and *E. coli* conducted differently with respect to both, ammonium depletion and increase of cellular N:C ratio. Displayed data (average ± average deviation) are based on 3–4 biological replicates. Strains were originally isolated from distant geographical provenances and disparate habitats. Detailed growth curves including substrate consumption profiles are provided in Fig. S3, Supporting Information.

S3, Supporting Information) may be used in an integrated yet presently unknown manner. The genes encoding these two nitrogen regulatory systems also co-occur in other roseobacters (Smith et al. 2013). In contrast, heterotrophic bacteria such as *E. coli* employ only the NtrBC/P_{II} system (van Heeswijk, Westerhoff and Boogerd 2013), whereas the oligotrophic marine bacterium ‘*Candidatus Pelagibacter ubique*’ relies exclusively on NtrXY (Smith et al. 2013).

With the depletion of external NH₄⁺, levels of most N-containing metabolites rapidly decreased in *P. inhibens* DSM 17395 (Fig. 3), until they were either strongly reduced in abundance or could not be detected during the stationary growth phase (at ≥50 h). Pronounced changes in cellular macromolecules were observed for DNA, RNA and proteins (Fig. 1), reflecting the elevated levels of the corresponding metabolite precursors (amino acids, nucleotides), as well as exponential growth (during NH₄⁺ depletion). The high demand for anabolic enzymes during NH₄⁺ assimilation (Fig. 4; Fig. S4 and Table S3, Supporting Information) may further contribute to the abundance increase of total proteins. The decrease in DNA, RNA and protein levels upon depletion of external NH₄⁺ paralleled the decreasing cellular N:C ratios (Fig. 1), and suggests degradation of these polymers to recycle polymer-bound nitrogen.

The copiously produced N-containing metabolites should distribute evenly in nitrogen-rich cells of *P. inhibens* DSM 17395 simply by diffusion, allowing for uniform propagation of cellular nitrogen from mother to daughter cells during cell division. Moreover, they serve as ‘prebuilt’ monomers for instantaneous polymer biosynthesis, especially during bulk growth after depletion of external NH₄⁺. The broad distribution of assimilated nitrogen into diverse cellular monomers and polymers

reveals an intuitive nitrogen storage strategy in *P. inhibens* DSM 17395. Most cyanobacteria as well as some heterotrophic bacteria respond to surplus nitrogen supply by specifically boosting the biosynthesis of arginine, as major building block for the nitrogen-rich storage polymer cyanophycin (multi-L-arginyl-poly-L-aspartate) generated by cyanophycin synthetase (Frommeyer, Wiefel and Steinbüchel 2016). Lacking genes for the latter, *P. inhibens* DSM 17395 cannot synthesize cyanophycin. *E. coli* responds to NH₄⁺ pulses (10 mM) by increasing the levels of several amino acids for a time span that was by far too short (≪ doubling time) to serve growth-relevant storage functions (Yuan et al. 2009). In contrast, the observed strategy of *P. inhibens* DSM 17395 to buildup surplus internal nitrogen stocks that fuel bulk growth more closely resembles that of eukaryotes. Marine phytoplankton internally stores nitrogen in the form of DNA, RNA, proteins or free amino acids, but also as NH₄⁺ or nitrate in vacuoles (Dortch et al. 1984; Admiraal, Peletier and Laane 1986).

High cellular nitrogen levels coincide with production of potential exotoxins and antibiotic TDA in *P. inhibens* DSM 17395

Phytoplankton-associated *P. inhibens* DSM 17395 is suggested to rely on secreted organic compounds (e.g. exoproteins, secondary metabolites) as important assets for its host-associated lifestyle (e.g. Porsby, Nielsen and Gram 2008; Seyedsayamdoost et al. 2011). The exoproteomes of diverse roseobacters (Christie-Oleza et al. 2012), including *P. inhibens* DSM 17395 (Kofsmehl et al. 2013), are dominated by potential RTX (Repeats-in-ToXin) proteins exported via type I secretion systems, also at hand in *P. inhibens* DSM 17395 (Kofsmehl et al. 2013). These toxins are

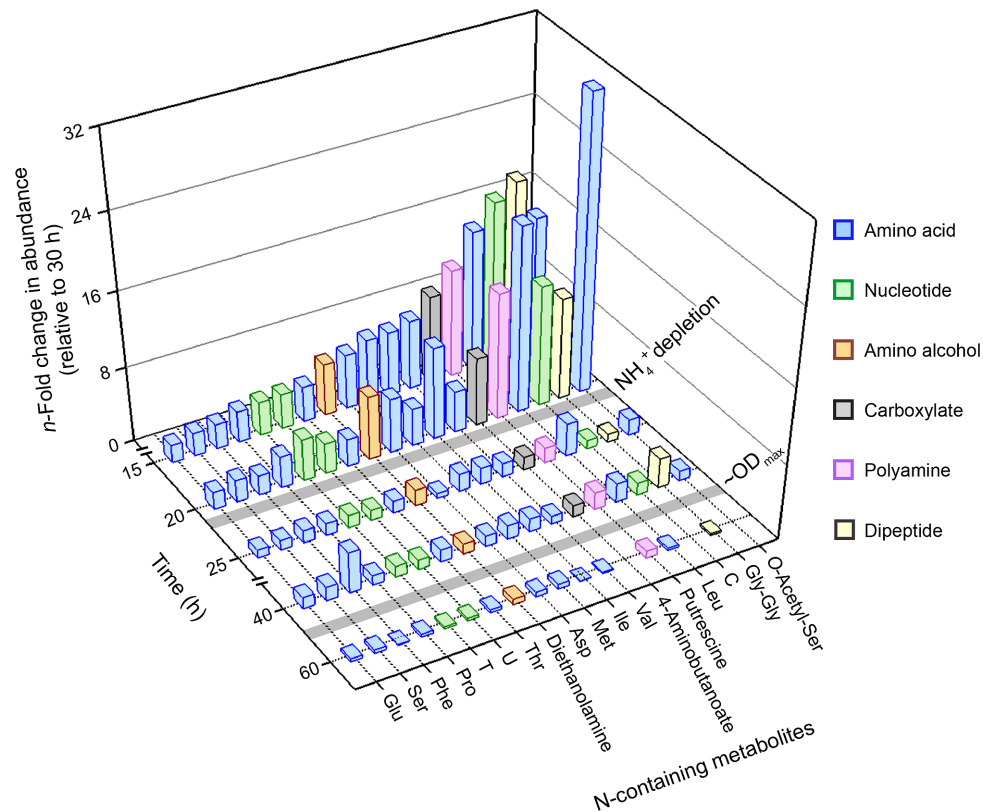


Figure 3. Abundance profile of intracellular N-containing metabolites detected during growth of *P. inhibens* DSM 17395 with 0.8 mM ammonium (see Fig. 1). For a complete list of detected metabolites see Table S4, Supporting Information. The grey bars (bottom plane) mark the time of ammonium depletion and the transit of cultures into stationary growth phase ($\sim OD_{max}$). Displayed data are based on the average of 5–6 biological replicates.

active against prokaryotic and eukaryotic cells, and have been suggested, amongst others, to form ion-permeable channels, thus dissipating ion gradients and the membrane potential (Linhartová et al. 2010). However, the actual mode of action of RTX-like proteins in roseobacters is currently unknown. In addition, *P. inhibens* DSM 17395 and related species produce the secondary metabolite TDA (e.g. Berger et al. 2011), which exhibits broad-spectrum antibiotic activity (Wilson et al. 2016). Here, we show that formation and maximal abundance of several potential RTX proteins and of TDA co-occur with high cellular N:C ratios buildup during depletion of external NH_4^+ (Fig. 5).

The most abundant of the eight identified potential RTX proteins (PGA1.65p00350) accounted for $\sim 50\%$ – 60% of the total SDS PAGE-resolvable exoproteome during NH_4^+ consumption and was estimated to reach maximal concentrations of $\sim 600 \mu g$ protein L^{-1} in the prepared exoproteome upon complete NH_4^+ depletion (Fig. S6, Supporting Information). The peak in production of this protein ($\sim 7 \mu g$ RTX protein per mg CDW) (Fig. 5a) was observed at highest cellular N:C ratios, which occurred before NH_4^+ depletion (Fig. 1b). We estimate that biosynthesis of this single RTX-like protein (molar N:C ratio of 0.32) at the observed concentrations should consume up to $\sim 1.0\%$ ($7\text{--}8 \mu M$) of the initially supplied NH_4^+ . With decreasing N:C ratios, the level of PGA1.65p00350 decreased continuously and reached almost zero in late stationary growth phase. The concentration profile of PGA1.65p00350 deviated strongly from that of the total exoproteins after NH_4^+ depletion (Fig. 5a), agreeing with the altered composition of the SDS PAGE-resolved total exoproteome (Fig. S6, Supporting Information). The decline in total

exoprotein abundance at $\sim OD_{max}$ coincided with the appearance of four secreted proteases/peptidases, possibly involved in external proteolysis of the excreted potential RTX and other proteins formed beforehand (Fig. S6, Supporting Information). Several identified amino acid- and peptide-specific transporters (Table S3, Supporting Information) potentially scavenge the proteolytic products for intracellular recycling of organic nitrogen during nitrogen starvation.

TDA levels in culture supernatants were measured indirectly by photometric detection of the diagnostic brown-colored TDA-iron complexes (Prol García et al. 2014; D’Alvise et al. 2015). As observed for PGA1.65p00350, maximal production of TDA was recorded at highest cellular N:C ratios and decreased after NH_4^+ was completely depleted (Fig. 5b). The TDA molecule itself does not contain nitrogen, but its biosynthesis drains N-containing intracellular metabolites (Phe, Cys) and requires specific enzymes (Fig. 4). This is evident from the higher abundance of biosynthetically relevant key metabolites (e.g. O-acetylserine) and enzymes (e.g. Tda proteins) during maximal TDA production (Figs. 4 and 5b). These results suggest that the metabolic status (levels of cellular nitrogen/amino acids) triggers the onset and duration of TDA formation irrespective of the initially supplied NH_4^+ concentration (0.4, 0.8 or 1.8 mM) (Fig. 1b; Figs. S1 and S7, Supporting Information). This link was not recognized previously owing to *P. inhibens* DSM 17395 being routinely cultured with nitrogen-rich complex media, which supported continuous TDA production during active growth (e.g. Berger et al. 2011; Trautwein et al. 2016). Moreover, integration of metabolic and quorum sensing signals (e.g. Berger et al. 2011; Prol García,

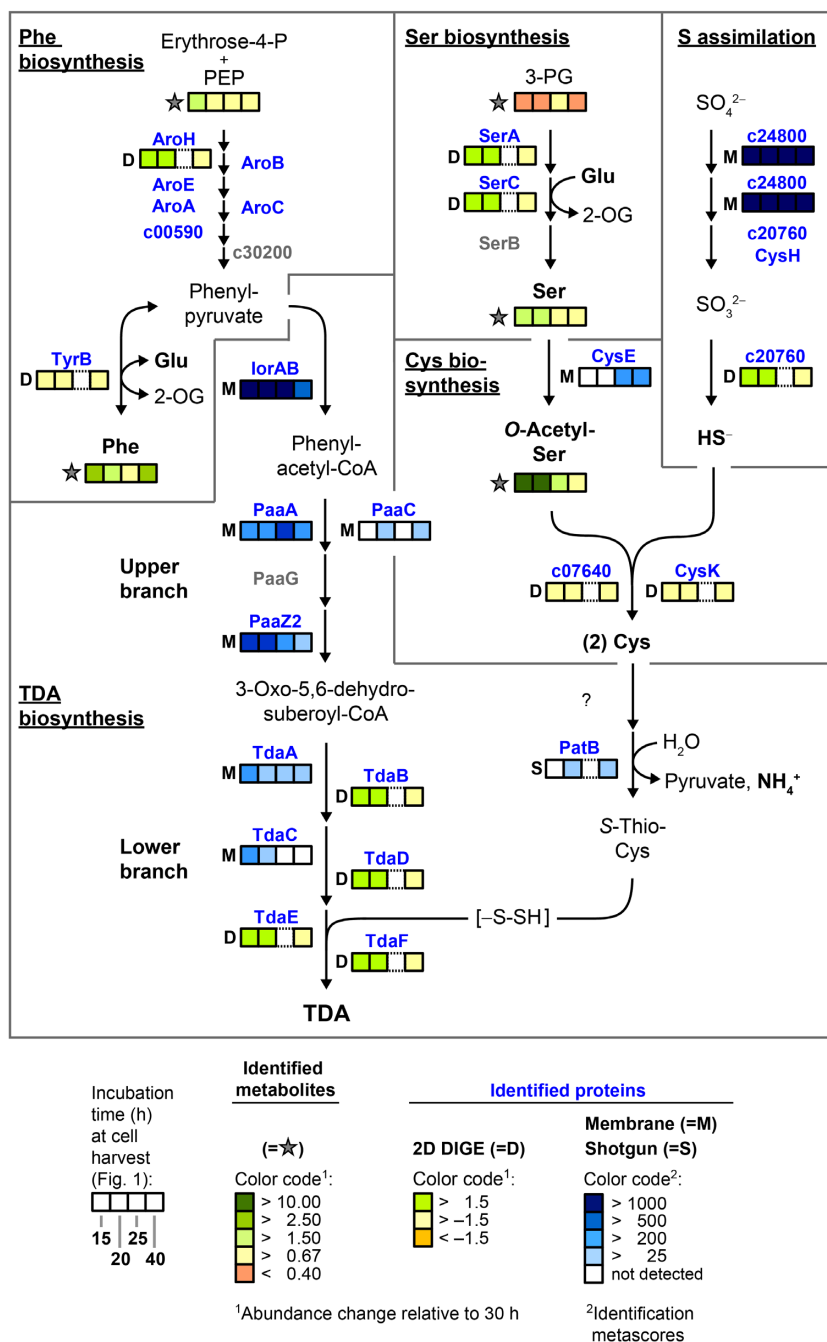


Figure 4. Biosynthesis of antibiotic TDA during ammonium depletion in *P. inhibens* DSM 17395 (see Fig. 5b). TDA biosynthesis is closely intertwined with the biosynthesis of amino acids (Phe, Ser, Cys) and with assimilatory sulfate reduction, thus requiring an integrated cross-regulation of carbon, nitrogen and sulfur metabolism in *P. inhibens* DSM 17395. TDA biosynthesis drains phenylpyruvate from Phe anabolism, proceeding via the conventional shikimate-chorismate pathway. Phenylpyruvate-derived phenylacetyl-CoA is then transformed via epoxidation and isomerization (oxepin-CoA forming), followed by ring cleavage to 3-oxo-5,6-dehydrosuberoyl-CoA (Teufel et al. 2011). The latter has been proposed to be converted to the seven-membered tropone carbocycle, ultimately receiving reduced sulfur from cysteine-derived S-thiocysteine (Brock, Nikolay and Dickschat 2014). Boxes indicate the time points (15, 20, 25, and 40 h; Fig. 1) for cell harvesting and their different colors reflect (i) relative changes in abundance of identified metabolites and soluble proteins (D; determined by 2D DIGE), as well as (ii) identification metascoring for soluble (S; determined by shotgun analysis) and membrane (M) proteins. The complete dataset is presented in Fig. S8, Supporting Information. Compound abbreviations in alphabetic order: 2-OG, 2-oxoglutarate; PEP, phosphoenolpyruvate; 3-PG, 3-phosphoglycerate; TDA, tropodithietic acid. Enzyme names in alphabetic order (identified: blue font color; predicted: grey font color): AroA, 3-phosphoshikimate-1-carboxyvinyltransferase; AroB, 3-hydroquinate synthase; AroC, chorismate synthase; AroE, shikimate dehydrogenase; AroH, phospho-2-dehydro-3-deoxyheptanoate aldolase; CysE, serine acetyltransferase; CysH, phosphoadenosine phosphosulfate reductase; CysK, cysteine synthase; IorAB, indolepyruvate oxidoreductase; PaaACG, proteins involved in phenylacetate degradation; PaaZ2, oxepin-CoA hydrolase/3-oxo-5,6-dehydrosuberoyl-CoA semialdehyde dehydrogenase (NADP⁺); PatB, cystathionine beta-lyase; PGA1.c00590, chorismate mutase; PGA1.c07640, O-acetylserine sulfhydrylase; PGA1.c20760, putative nitrite/sulfite reductase; PGA1.c24800, putative bifunctional SAT/APS kinase; PGA1.c30200, prephenate dehydratase; SerA, 3-phosphoglycerate dehydrogenase; SerB, phosphoserine phosphatase; SerC, phosphoserine aminotransferase; TdaA, transcriptional regulator, LysR family; TdaB, putative beta etherase; TdaC, conserved hypothetical protein, similar to prephenate dehydratase; TdaD, thioesterase superfamily protein; TdaE, acyl-CoA dehydrogenase; TdaF, putative flavoprotein, HFCD family; TyrB, aromatic amino acid aminotransferase.

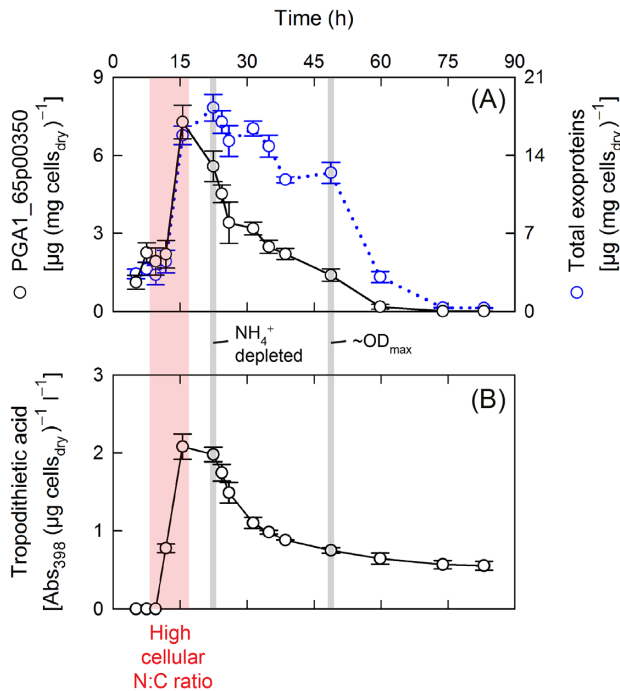


Figure 5. Nitrogen-dependent secretion of exoproteins and TDA by *P. inhibens* DSM 17395 during growth with 0.8 mM ammonium (see Fig. 1). Production of (A) the abundant potential RTX protein PGA1.65p00350 in comparison to the total exoproteins (for details see Fig. S6, Supporting Information) and of (B) the antibiotic secondary metabolite TDA, draining amino acids during its biosynthesis (see Fig. 4). TDA was determined indirectly by its absorbance at 398 nm (Abs_{398}). Displayed data (average \pm average deviation) are based on 3–4 biological replicates.

D’Alvise and Gram 2013) could contribute to the higher maximal levels of TDA during growth with excess of nitrogen (Fig. S7, Supporting Information). High cellular N:C ratios apparently also positively influence toxin production in marine phytoplankton (Camargo and Alonso 2006).

Ecological implications

Heterotrophic bacteria are essential drivers of the nitrogen cycle in the oceans, amongst others by regenerating NH_4^+ during the mineralization of biomass and/or competing with phytoplankton for its utilization. The efficient sequestering of NH_4^+ appears to be useful for *P. inhibens* DSM 17395 and related strains (Fig. 2) in several ways: (i) internal (‘private’) reservoirs exclusively benefit their descendants, (ii) competing bacterioplankton (including ammonia-oxidizing archaea and bacteria (Martens-Habben et al. 2009)) and phytoplankton species could be deprived of this nutrient, and (iii) it could prevent competitors from potentially growing faster. The capacity to rapidly store nitrogen internally possibly reflects the strong influence of NH_4^+ availability on the growth of *P. inhibens* DSM 17395 (Trautwein et al. 2017) and in more general terms an adaptation to fluctuating NH_4^+ supply. The latter is expected to occur frequently in the natural habitat of the studied roseobacters: on a larger scale in coastal regions and on a microcosm-scale on marine snow particles representing nutrient-rich hotspots in otherwise oligotrophic water columns (Azam and Long 2001; Gram et al. 2002). To extrapolate these new findings for *P. inhibens* DSM 17395 and its close relatives from this defined study to the natural environment is, of course, speculative at present, since *in situ* concentrations of

NH_4^+ vary considerably, and nutrient supply (incl. various nitrogen sources from DIN and DON) as well as community composition are much more complex.

Investing the costly acquired nitrogen at the right time into massive secretion of potential RTX proteins, as well as into the complex biosynthesis of TDA (Figs. 4 and 5), may be part of a defense mechanism in *P. inhibens* DSM 17395 from predation and aggressive displacement from colonized nutritional hotspots (e.g. algae, rotifers, fish larvae) by competing species. Restricting maximal production of potential RTX proteins and TDA to nitrogen-rich cells implies that eukaryotic interaction partners could benefit even longer from protection against pathogens (e.g. *Vibrio* sp.), if they continuously provide *P. inhibens* DSM 17395 with sufficient amounts of reduced nitrogen. N_2 -fixing phytoplankton constantly release N-containing metabolites (mainly free amino acids) (Mague et al. 1980; Sarmiento et al. 2013), which increases even more under inorganic nutrient limitation when internal carbon storage capacities are exceeded (Obernosterer and Herndl 1995; Wilhelm et al. 2006). During growth of *P. inhibens* DSM 17395 with an excessive supply of nitrogen provided by a complex medium rich in amino acids and resembling the composition of phytoplankton exudates, the organism simultaneously utilized most of the amino acids, sustained a high cellular N:C ratio and continuously produced potential RTX proteins and TDA until OD_{max} (Zech et al. 2013b; Trautwein et al. 2016). Reduced (in)organic nitrogen could thus play a key role in fostering the proposed mutually beneficial interactions between *P. inhibens* DSM 17395 and phytoplankton (Seyedsayamdost et al. 2011).

CONCLUSIONS

Phaeobacter inhibens DSM 17395 exploits external NH_4^+ in a complex manner throughout the different stages of growth that starts with (i) the transient buildup of diverse intracellular nitrogen reservoirs to facilitate rapid depletion and assimilation of external NH_4^+ during early growth (Fig. 6), followed by (ii) propagation and redistribution of intracellular nitrogen during bulk growth accompanied by carbon (PHB) storage (Fig. 1), and finally (iii) breakdown and recycling of DNA, RNA and proteins (internal and secreted) during nitrogen starvation in the stationary growth phase (Supplementary Results and Discussion). The allocation of assimilated nitrogen into monomeric and polymeric cellular constituents for transient nitrogen storage (Fig. 6) appears intuitive, but should come with high energetic costs for boosted global production of the many biosynthetic enzymes required, and for biosynthesis itself. This contrasts the metabolically much simpler way of nitrogen storage in bacteria producing a homogeneous N-reserve polymer such as cyanophycin. Instead, the nitrogen storage strategy of *P. inhibens* DSM 17395 resembles that of eukaryotic phytoplankton and may reveal another facet of an apparently close relationship between a heterotrophic bacterioplankton member and its eukaryotic interaction partners. Nitrogen-dependent secretion of potential RTX proteins and TDA (Fig. 5) could enable *P. inhibens* DSM 17395 to bequeath the secured nitrogen successfully to subsequent generations. Considering that biosynthesis of the antimicrobial secondary metabolite TDA occurs at the interface between amino acid biosynthesis and sulfur assimilation (Fig. 4), an integrated cross-regulation of C-, N- and S-metabolism in *P. inhibens* DSM 17395 seems likely. The rapid storage of nitrogen described for *Phaeobacter* spp. and *R. pomeroyi* may add a new facet to the

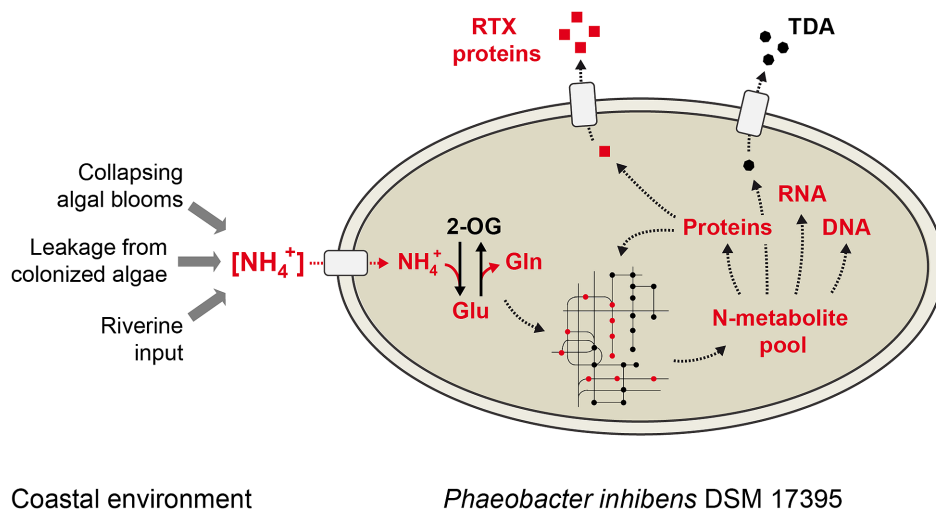


Figure 6. Schematic model of transitory nitrogen storage in *P. inhibens* DSM 17395. External ammonium, possibly derived from different environmental sources, is rapidly assimilated (via glutamate and glutamine) and utilized for biosynthesis of diverse N-containing metabolites and cellular macromolecules. Investing parts of the assimilated nitrogen in biosynthesis and secretion of potential RTX proteins and antibiotic TDA may ensure competitive nutrient acquisition and protection of nitrogen-rich cells from predation.

marine nitrogen cycle, as heterotrophic bacteria, like phytoplankton, may pursue a 'luxury goods' strategy, resulting in a transient intracellular accumulation of reduced nitrogen and conversely its removal from the readily accessible communal seawater pool.

SUPPLEMENTAL DATA

Supplementary data are available at FEMSEC online.

ACKNOWLEDGMENTS

We are grateful to M. Dörries, R. Gahl-Janssen, U. Maschmann, S. Scheeve and C. Versteegen (Oldenburg), D. Thies (Bremen), S. Kaltenhäuser (Braunschweig) and K. Kemper (Münster) for technical assistance and B. Fuchs (Bremen) for providing access to flow cytometer. We thank B. Golding (Newcastle) for valuable comments on the manuscript.

FUNDING

This study was supported by the Deutsche Forschungsgemeinschaft (SFB TRR 51).

Conflict of interest. None declared.

REFERENCES

- Azam F, Long RA. Sea snow microcosms. *Nature* 2001;**414**:495–8.
- Azam F, Malfatti F. Microbial structuring of marine ecosystems. *Nat Rev Microbiol* 2007;**5**:782–91.
- Admiraal W, Peletier H, Laane R. Nitrogen metabolism of marine planktonic diatoms; excretion, assimilation and cellular pools of free amino acids in seven species with different cell size. *J Exp Mar Biol Ecol* 1986;**98**:241–63.
- Beg QK, Zampieri M, Klitgord N et al. Detection of transcriptional triggers in the dynamics of microbial growth: application to the respiratorily versatile bacterium *Shewanella oneidensis*. *Nucleic Acids Res* 2012;**40**:7132–49.
- Berger M, Neumann A, Schulz S et al. Tropodithietic acid production in *Phaeobacter gallaeciensis* is regulated by N-acyl homoserine lactone-mediated quorum sensing. *J Bacteriol* 2011;**193**:6576–85.
- Boncompain G, Müller C, Meas-Yedid V et al. The intracellular bacteria *Chlamydia* hijack peroxisomes and utilize their enzymatic capacity to produce bacteria-specific phospholipids. *PLoS ONE* 2014;**9**:e86196.
- Bradford MM. A rapid and sensitive method for the quantitation of microgram quantities of protein utilizing the principle of protein-dye binding. *Anal Biochem* 1976;**72**:248–54.
- Brock NL, Nikolay A, Dickschat JS. Biosynthesis of the antibiotic tropodithietic acid by the marine bacterium *Phaeobacter inhibens*. *Chem Commun* 2014;**50**:5487–9.
- Buchan A, González JM, Moran MA. Overview of the marine *Roseobacter* lineage. *Appl Environ Microbiol* 2005;**71**:5665–77.
- Buchan A, LeCleir GR, Gulvik CA et al. Master recyclers: features and functions of bacteria associated with phytoplankton blooms. *Nat Rev Microbiol* 2014;**12**:686–98.
- Buddruhs N, Pradella S, Göker M et al. Molecular and phenotypic analyses reveal the non-identity of the *Phaeobacter gallaeciensis* type strain deposits CIP 105210^T and DSM 17395. *Int J Syst Evol Microbiol* 2013;**63**:4340–9.
- Camargo JA, Alonso Á. Ecological and toxicological effects of inorganic nitrogen pollution in aquatic ecosystems: A global assessment. *Environ Int* 2006;**32**:831–49.
- Caspi R, Billington R, Ferrer L et al. The MetaCyc database of metabolic pathways and enzymes and the BioCyc collection of pathway/genome databases. *Nucleic Acids Res* 2016;**44**:D471–80.
- Chaney AL, Marbach EP. Modified reagents for determination of urea and ammonium. *Clin Chem* 1962;**8**:130–2.
- Chang A, Schomburg I, Placzek S et al. BRENDA in 2015: exciting developments in its 25th year of existence. *Nucleic Acids Res* 2015;**43**:D439–46.
- Christie-Oleza JA, Piña-Villalonga JM, Bosch R et al. Comparative proteogenomics of twelve *Roseobacter* exoproteomes reveals different adaptive strategies among these marine bacteria. *Mol Cell Proteomics* 2012;**11**:1–12.
- Conroy MJ, Durand A, Lupo D et al. The crystal structure of the *Escherichia coli* AmtB-GlnK complex reveals how GlnK

- regulates the ammonia channel. *Proc Natl Acad Sci USA* 2007;**104**:1213–8.
- D'Alvise PW, Phippen CBW, Nielsen KF et al. Influence of iron on production of the antibacterial compound tropodithietic acid and its noninhibitory analog in *Phaeobacter inhibens*. *Appl Environ Microbiol* 2015;**82**:502–9.
- Doherty NS, Littman BH, Reilly K et al. Analysis of changes in acute-phase plasma proteins in an acute inflammatory response and in rheumatoid arthritis using two-dimensional gel electrophoresis. *Electrophoresis* 1998;**19**:355–63.
- Dortch Q, Clayton JR, Jr, Thoresen SS et al. Species differences in accumulation of nitrogen pools in phytoplankton. *Mar Biol* 1984;**81**:237–50.
- Droop MR. Vitamin B12 and marine ecology. IV. The kinetics of uptake, growth and inhibition in *Monochrysis lutheri*. *J Mar Biol Ass UK* 1968;**48**:689–733.
- Drüppel K, Hensler M, Trautwein K et al. Pathways and substrate-specific regulation of amino acid degradation in *Phaeobacter inhibens* DSM 17395 (archetype of the marine *Roseobacter* clade). *Environ Microbiol* 2014;**16**:218–38.
- Duguid JP, Wilkinson JF. The influence of cultural conditions on polysaccharide production by *Aerobacter aerogenes*. *J Gen Microbiol* 1953;**9**:174–89.
- Fagerbakke KM, Heldal M, Norland S. Content of carbon, nitrogen, oxygen, sulfur and phosphorus in native aquatic and cultured bacteria. *Aquat Microb Ecol* 1996;**10**:15–27.
- Falkowski P, Barber R, Smetacek V. Biogeochemical controls and feedbacks on ocean primary production. *Science* 1998;**281**:200–6.
- Field C, Behrenfeld M, Randerson J et al. Primary production of the biosphere: integrating terrestrial and oceanic components. *Science* 1998;**281**:237–40.
- Frommeyer M, Wiefel L, Steinbüchel A. Features of the biotechnologically relevant polyamide family 'cyanophycins' and their biosynthesis in prokaryotes and eukaryotes. *Crit Rev Biotechnol* 2016;**36**:153–64.
- Gade D, Thiermann J, Markowsky D et al. Evaluation of two-dimensional difference gel electrophoresis for protein profiling. *J Mol Microbiol Biotechnol* 2003;**5**:240–51.
- Goldman JC, Dennett MR. Ammonium regeneration and carbon utilization by marine bacteria grown on mixed substrates. *Marine Biol* 1991;**109**:369–78.
- Goldman JC, Dennett MR. Rapid nitrogen uptake by marine bacteria. *Limnol Oceanogr* 2001;**46**:1195–8.
- Görg A, Weiss W, Dunn MJ. Current two-dimensional electrophoresis technology for proteomics. *Proteomics* 2004;**4**:3665–85.
- Gram L, Grossart H-P, Schlingloff A et al. Possible quorum sensing in marine snow bacteria: production of acylated homoserine lactones by *Roseobacter* strains isolated from marine snow. *Appl Environ Microbiol* 2002;**68**:4111–6.
- Gram L, Rasmussen BB, Wemheuer B et al. *Phaeobacter inhibens* from the *Roseobacter* clade has an environmental niche as a surface colonizer in harbors. *Syst Appl Microbiol* 2015;**38**:483–93.
- Guevara-Martinez M, Sjöberg Gällnö K, Sjöberg G et al. Regulating the production of (R)-3-hydroxybutyrate in *Escherichia coli* by N or P limitation. *Front Microbiol* 2015;**6**:844.
- Hiller K, Hangebrauk J, Jäger C et al. MetaboliteDetector: comprehensive analysis tool for targeted and nontargeted GC/MS based metabolome analysis. *Anal Chem* 2009;**81**:3429–39.
- Horiuchi T. RNA degradation and DNA and protein synthesis of *E. coli* B. in a phosphate deficient medium. *J Biochem* 1959;**46**:1467–79.
- Ingber L. Very fast simulated re-annealing. *Math Comput Model* 1989;**12**:967–73.
- Kirchman DL. The uptake of inorganic nutrients by heterotrophic bacteria. *Microb Ecol* 1994;**28**:255–71.
- Kleiner D. Bacterial ammonium transport. *FEMS Microbiol Rev* 1985;**32**:87–100.
- Koßmehl S, Wöhlbrand L, Drüppel K et al. Subcellular protein localization (cell envelope) in *Phaeobacter inhibens* DSM 17395. *Proteomics* 2013;**13**:2743–60.
- Laws EA, Falkowski PG, Smith WO et al. Temperature effects on export production in the open ocean. *Global Biogeochem Cycles* 2000;**14**:1231–46.
- Li Y, Schichtel BA, Walker JT et al. Increasing importance of deposition of reduced nitrogen in the United States. *Proc Natl Acad Sci USA* 2016;**113**:5874–9.
- Linhartová I, Bumba K, Mašín J et al. RTX proteins: a highly diverse family secreted by a common mechanism. *FEMS Microbiol Rev* 2010;**34**:1076–12.
- Lowry OH, Rosebrough NJ, Farr AL et al. Protein measurement with the folin phenol reagent. *J Biol Chem* 1951;**193**:265–75.
- Luo H, Moran MA. Evolutionary ecology of the marine *Roseobacter* clade. *Microbiol Mol Biol Rev* 2014;**78**:573–87.
- Luo H, Swan BK, Stepanauskas R et al. Evolutionary analysis of a streamlined lineage of surface ocean *Roseobacters*. *ISME J* 2014;**8**:1428–39.
- Mague TH, Friberg E, Hughes DJ et al. Extracellular release of carbon by marine phytoplankton; a physiological approach. *Limnol Oceanogr* 1980;**25**:262–79.
- Martens-Habbena W, Berube PM, Urakawa H et al. Ammonia oxidation kinetics determine niche separation of nitrifying archaea and bacteria. *Nature* 2009;**461**:976–9.
- Matyash V, Liebisch G, Kurzchalia TV et al. Lipid extraction by methyl-tert-butyl ether for high-throughput lipidomics. *J Lipid Res* 2008;**49**:1137–46.
- Monod J. *Recherches sur la croissance des cultures bactériennes*, Hermann & Cie, Paris, France 1942.
- Obernosterer I, Herndl GJ. Phytoplankton extracellular release and bacterial growth: dependence on the inorganic N:P ratio. *Mar Ecol Prog Ser* 1995;**116**:247–57.
- Oldenhuis R, Vandekerckhove J. GODLIKE—a robust single- and multi-objective optimizer. *Matlab Central* 2009.
- Porsby CH, Nielsen KF, Gram L. *Phaeobacter* and *Ruegeria* species of the *Roseobacter* clade colonize separate niches in a Danish Turbot (*Scophthalmus maximus*)-rearing farm and antagonize *Vibrio anguillarum* under different growth conditions. *Appl Environ Microbiol* 2008;**74**:7356–64.
- Prol García MJ, D'Alvise PW, Gram L. Disruption of cell-to-cell signaling does not abolish the antagonism of *Phaeobacter galacensis* toward the fish pathogen *Vibrio anguillarum* in algal systems. *Appl Environ Microbiol* 2013;**79**:5414–7.
- Prol García MJ, D'Alvise PW, Rygaard AM et al. Biofilm formation is not a prerequisite for production of the antibacterial compound tropodithietic acid in *Phaeobacter inhibens* DSM 17395. *J Appl Microbiol* 2014;**117**:1592–600.
- Redfield AC. The biological control of chemical factors in the environment. *Am Sci* 1958;**46**:205–21.
- Ruppersberg HS, Goebel MR, Kleinert SI et al. Photometric determination of ammonium and phosphate in seawater medium using a microplate reader. *J Mol Microbiol Biotechnol* 2017;**27**:73–80.
- Saier MH, Reddy VS, Tsu BV et al. The transporter classification database (TCDB): recent advances. *Nucleic Acids Res* 2016;**44**:D372–9.

- Sambrook J, Russell DW. *Molecular Cloning: A Laboratory Manual*, Cold Spring Harbor, NY: Cold Spring Harbor Laboratory, 2001.
- Sarmiento H, Romera-Castillo C, Lindh M et al. Phytoplankton species-specific release of dissolved free amino acids and their selective consumption by bacteria. *Limnol Oceanogr* 2013;**58**:1123–35.
- Segev E, Wyche TP, Kim KH et al. Dynamic metabolic exchange governs a marine algal-bacterial interaction. *elife* 2016;**5**:514.
- Seyedsayamdost MR, Case RJ, Kolter R et al. The Jekyll-and-Hyde chemistry of *Phaeobacter gallaeciensis*. *Nat Chem* 2011;**3**:331–5.
- Smith DP, Thrash JC, Nicora CD et al. Proteomic and transcriptomic analyses of 'Candidatus Pelagibacter ubique' describe the first PII-independent response to nitrogen limitation in a free-living Alphaproteobacterium. *mBio* 2013;**4**:e00133–12.
- Storn R, Price K. Differential evolution – a simple and efficient heuristic for global optimization over continuous spaces. *J Global Optim* 1997;**11**:341–59.
- Suhre K, Schmitt-Kopplin P. MassTRIX: mass translator into pathways. *Nucleic Acids Res* 2008;**36**:W481–4.
- Teeling H, Fuchs BM, Becher D et al. Substrate-controlled succession of marine bacterioplankton populations induced by a phytoplankton bloom. *Science* 2012;**336**:608–11.
- Teufel R, Gantert C, Voss M et al. Studies on the mechanism of ring hydrolysis in phenylacetate degradation: a metabolic branching point. *J Biol Chem* 2011;**286**:11021–34.
- Thole S, Kalhoefer D, Voget S et al. *Phaeobacter gallaeciensis* genomes from globally opposite locations reveal high similarity of adaptation to surface life. *ISME J* 2012;**6**:2229–44.
- Thomas G, Coutts G, Merrick M. The *glnKamtB* operon. A conserved gene pair in prokaryotes. *Trends Genet* 2000;**16**:11–4.
- Trautwein K, Feenders C, Hulsch R et al. Non-Redfield, nutrient synergy, and flexible internal elemental stoichiometry in a marine bacterium. *FEMS Microbiol Ecol* 2017;**93**:fix059
- Trautwein K, Kühner S, Wöhlbrand L et al. Solvent stress response of the denitrifying bacterium 'Aromatoleum aromaticum' strain EbN1. *Appl Environ Microbiol* 2008;**74**:2267–74.
- Trautwein K, Lahme S, Wöhlbrand L et al. Physiological and proteomic adaptation of 'Aromatoleum aromaticum' EbN1 to low growth rates in benzoate-limited, anoxic chemostats. *J Bacteriol* 2012;**194**:2165–80.
- Trautwein K, Will SE, Hulsch R et al. Native plasmids restrict growth of *Phaeobacter inhibens* DSM 17395: Energetic costs of plasmids assessed by quantitative physiological analyses. *Environ Microbiol* 2016;**18**:4817–29.
- Van de Waal DB, Ferreruela G, Tonk L et al. Pulsed nitrogen supply induces dynamic changes in the amino acid composition and microcystin production of the harmful cyanobacterium *Planktothrix agardhii*. *FEMS Microbiol Ecol*, 2010;**74**:430–8.
- van Heeswijk WC, Westerhoff HV, Boogerd FC. Nitrogen assimilation in *Escherichia coli*: putting molecular data into a systems perspective. *Microbiol Mol Biol Rev* 2013;**77**:628–95.
- Wagner-Döbler I, Biebl H. Environmental biology of the marine *Roseobacter* lineage. *Annu Rev Microbiol* 2006;**60**:255–80.
- Wanner U, Egli T. Dynamics of microbial growth and cell composition in batch culture. *FEMS Microbiol Rev* 1990;**75**:19–44.
- Wheeler PA, Kirchman DL. Utilization of inorganic and organic nitrogen by bacteria in marine systems. *Limnol Oceanogr* 1986;**31**:998–1009.
- Wilhelm C, Büchel C, Fisahn J et al. The regulation of carbon and nutrient assimilation in diatoms is significantly different from green algae. *Protist* 2006;**157**:91–124.
- Wilson MZ, Wang R, Gitai Z et al. Mode of action and resistance studies unveil new roles for tropodithietic acid as an anti-cancer agent and the γ -glutamyl cycle as a proton sink. *Proc Natl Acad Sci USA* 2016;**113**:1630–5.
- Yuan J, Doucette CD, Fowler WU et al. Metabolomics-driven quantitative analysis of ammonia assimilation in *E. coli*. *Mol Syst Biol* 2009;**5**:302.
- Zech H, Thole S, Schreiber K et al. Growth phase-dependent global protein and metabolite profiles of *Phaeobacter gallaeciensis* strain DSM 17395, a member of the marine *Roseobacter*-clade. *Proteomics* 2009;**9**:3677–97.
- Zech H, Hensler M, Koßmehl S et al. Adaptation of *Phaeobacter inhibens* DSM 17395 to growth with complex nutrients. *Proteomics* 2013a;**13**:2851–68.
- Zech H, Hensler M, Koßmehl S et al. Dynamics of amino acid utilization in *Phaeobacter inhibens* DSM 17395. *Proteomics* 2013b;**13**:2869–85.
- Zehr JP, Kudela RM. Nitrogen cycle of the open ocean: from genes to ecosystems. *Annu Rev Marine Sci* 2011;**3**:197–225.